Atom probe tomography today

This review aims to describe and illustrate the advances in the application of atom probe tomography that have been made possible by recent developments, particularly in specimen preparation techniques (using dual-beam focused-ion beam instruments) but also of the more routine use of laser pulsing. The combination of these two developments now permits atomic-scale investigation of site-specific regions within engineering alloys (e.g. at grain boundaries and in the vicinity of cracks) and also the atomic-level characterization of interfaces in multilayers, oxide films, and semiconductor materials and devices.

Alfred Cerezo*[a,b], Peter H. Clifton[c], Mark J. Galtrey[d], Colin J. Humphreys[d], Thomas F. Kelly[c], David J. Larson[c], Sergio Lozano-Perez[b], Emmanuelle A. Marquis[a,b], Rachel A. Oliver[d], Gang Sha[b], Keith Thompson[c], Mathijs Zandbergen[b], and Roger L. Alvis[c]

[a]*Opal UK National Atom Probe Facility*

[b]*Department of Materials, University of Oxford, Parks Road, Oxford, OX1 3PH, UK*

[c]*Imago Scientific Instruments, 5500 Nobel Drive, Madison, WI 53711, USA*

[d]*Department of Materials Science and Metallurgy, University of Cambridge, Pembroke Street, Cambridge, CB2 3QZ, UK*

**E-mail: alfred.cerezo@materials.oxford.ac.uk*

For much of its 40 year history, atom probe field-ion microscopy[1] has been an esoteric scientific technique, practiced in only a score of academic laboratories worldwide. Many materials scientists knew of it, but few had ever used an atom probe. The development of the three-dimensional atom probe (3DAP) expanded the technique, and gave tremendous capabilities for three-dimensional compositional imaging with high analytical sensitivity at the atomic scale[2–4]. However, the number of users of atom probe tomography (APT) remained small for several important reasons: the instrument required a sharp needle-shaped specimen, which can be difficult to produce; the specimen had to have good electrical conductivity for voltage-pulsed field evaporation; images came from very small volumes and took a long time to obtain (~10^4 nm^3 per day); and it was very difficult to isolate specific features of interest in a bulk material for analysis. In the past five years, these constraints have been largely overcome by a combination of developments in focused-ion beam (FIB) technology and commercially available 3DAP instruments that are reliable and easy to use.

FIB instruments can now be used to selectively extract micron-sized pieces from metal alloys and semiconductor devices and sharpen them for APT[5,6]. The use of laser-pulsed field evaporation in APT has made it possible to analyze materials with much lower electrical conductivity and even thin films of insulating oxides[7–9]. Larger sample volumes (>100 nm diameter by 500 nm long cylinders) are now analyzed at high data collection rates (>10^6 nm^3 per day.) These improvements

ISSN:1369 7021 © Elsevier Ltd 2007

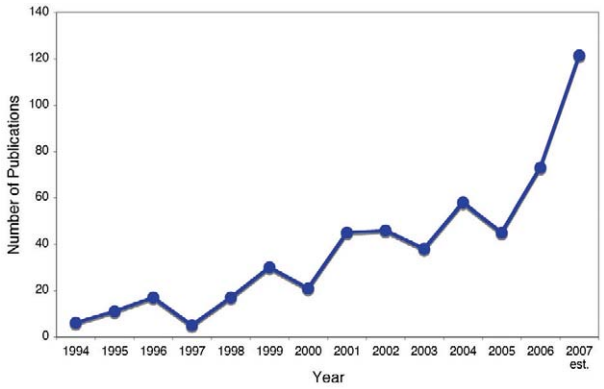

Fig. 1 The number of scientific publications worldwide on APT since 1994, showing a recent sharp upturn to the steady growth in numbers over the years. Data were obtained from Web of Science and show the number of papers containing any of the following terms in the title, abstract, or keywords: atom probe tomography, tomographic atom probe, three- (or 3-) dimensional atom probe, 3DAP. The figure for 2007 is estimated, based on the 91 papers published up to the end of September.

have made the technique attractive to a much broader audience. New APT laboratories have been established around the world, and user facilities have been created (such as those at Oak Ridge National Laboratory[10] and Northwestern University[11] in the US and the Opal facility in the UK[12]) to cater for nonspecialists. This expansion of the user-base has contributed to a recent sharp upturn in the steady growth of scientific publications within the field over the past few years (Fig. 1).

The unique capability of APT to identify and quantify individual chemical species in three dimensions is fast becoming a requirement for atomic level microscopy. The technique is a natural complement to other major microscopy techniques such as transmission electron microscopy (TEM) and secondary ion mass spectrometry (SIMS), but APT provides the highest available spatial resolution for chemical analysis. Well-equipped laboratories studying nanoscale phenomena will find APT has become an essential tool. The key to expanding the materials science problems accessible to APT has been, and will continue to be, the ability to craft specimens from a wide spectrum of materials in their as-available state. The development of 'lift-out' techniques using a dual-beam FIB to extract site-specific specimens for analysis has greatly improved sampling productivity and made possible a whole raft of new APT studies. This review describes the essence of recent developments, with illustrations selected from engineering alloy and semiconductor applications.

How the atom probe works

The atom probe combines a time-of-flight mass spectrometer with a point projection microscope capable of atomic-scale imaging[13]. Combining this with position sensing in the 3DAP (Fig. 2) permits the full three-dimensional reconstruction capabilities of APT. By applying a high voltage (~10 kV), a high electric field (~10^{10} V/m) is created

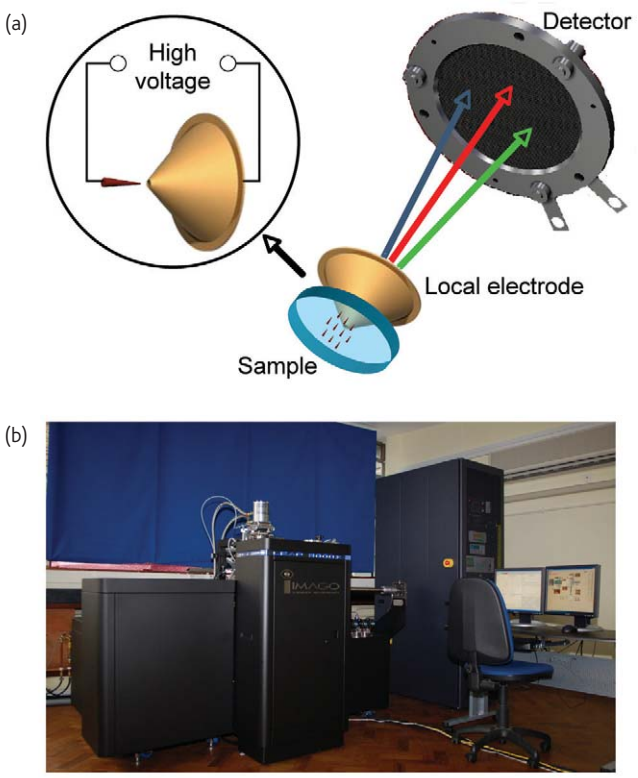

Fig. 2 (a) Schematic of a three-dimensional local electrode atom probe. The atoms are field evaporated from the apex of a needle-shaped specimen by application of a high electric field between the counter (local) electrode and the specimen (see inset). The ions fly toward an imaging detector and their hit position is a direct mapping of the original atomic positions on the specimen. (b) View of the LEAP™ 3000XSi instrument at the Opal facility in Oxford.

on the apex of a sharp (<100 nm radius) specimen held at cryogenic temperatures. Applying the voltage between the specimen and a local electrode[14,15], as in the local electrode atom probe (LEAP) in Fig. 2, allows the field to be applied selectively to a single specimen in an array of microtips. Atoms on the specimen apex are field evaporated as ions and accelerated toward the imaging detector. By pulsing the evaporation, e.g. by using subnanosecond voltage pulses in addition to the dc voltage, the flight time of each ion can be measured and used to calculate the mass-to-charge ratio and thus determine its chemical nature. The ~100 nm diameter area on the apex is projected onto the roughly 100 mm diameter detector, giving a magnification of 10^6. The original position of atoms on the specimen apex is determined from the hit position of the ions on the detector, while the sequence of evaporation events is used to provide depth information. This combination of data allows three-dimensional images of the element distributions to be reconstructed with near-atomic resolution.

The high spatial resolution elemental mapping capability of APT has made it invaluable in the study of ultrafine-scale precipitate distributions in metallic alloys, which until recently has been the main application of the technique. As an example of the results that can be obtained, Fig. 3 shows an aging sequence in a 6xxx series Al alloy.

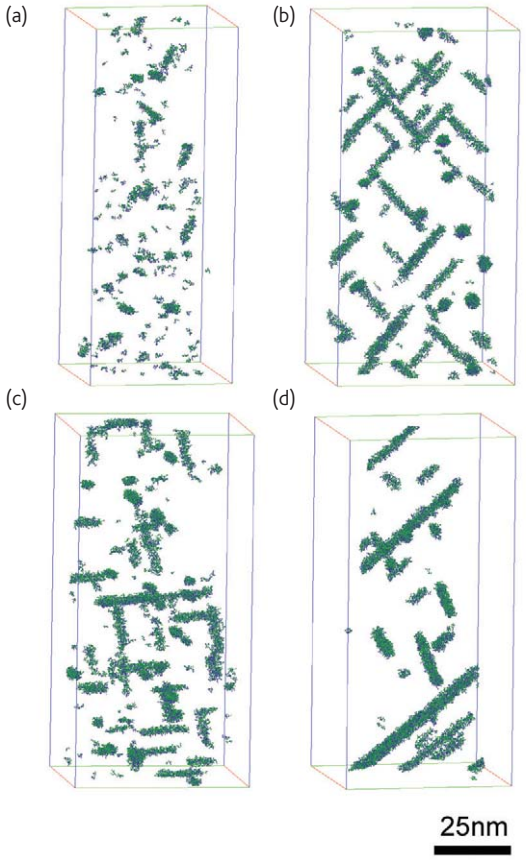

Fig. 3. Atom maps showing the three-dimensional elemental distributions of Mg (green) and Si (blue) from within the precipitates in an Al–0.5 wt.% Mg–1.0 wt.% Si alloy aged at 180°C for (a) 10 mins, (b) 30 mins, (c) 4 hrs, and (d) 18 hrs. The images show the development of the elongated (001)-oriented β″ phase that produces marked precipitation hardening in this alloy.

These alloys are used as body-sheet materials for automobiles because of their low weight and relatively high strength. During artificial aging at 180°C, an increase in strength is seen in these alloys through precipitation hardening. The precipitation sequence is: supersaturated solution → Mg-Si co-clusters → small precipitates (GP zones) → β'' → β' → β. The APT images in Fig. 3 show the distribution of Mg and Si atoms within precipitates (as selected by the maximum separation method[16]) from an Al–0.5 wt% Mg–1.0 wt% Si alloy aged at 180°C for different times. Elongated β'' precipitates, which form the main strengthening phase, can be seen growing along the <100> directions. The ultrafine scale of these precipitates has made APT an important tool for worldwide studies of this class of alloys[17–20].

Laser-pulsed APT

Historically, voltage pulses have been used to generate pulsed field evaporation, but this requires that the specimen has high electrical conductivity (>10^2 S/cm), limiting the technique to metals (as above) and heavily doped semiconductors. However, short laser pulses (<1 ns) directed at the specimen apex can be used to induce a pulse

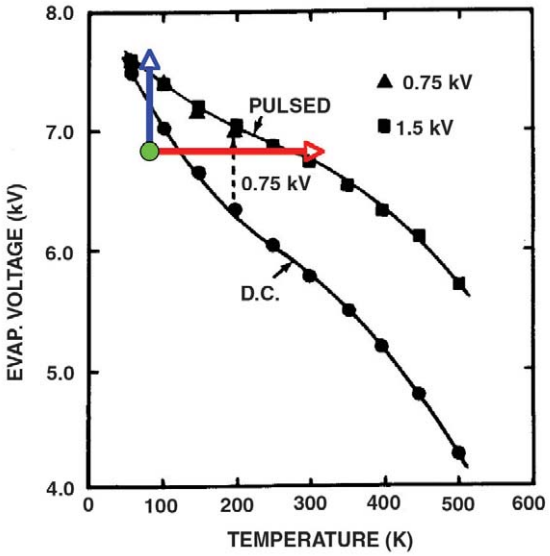

Fig. 4 Data showing the variation in voltage required for either dc or pulsed field evaporation of tungsten as a function of temperature. (Reprinted with permission from[22]. © 1981 American Institute of Physics.) From a voltage below that needed to generate dc field evaporation (green dot), pulsed-field evaporation can be generated either with a voltage pulse (blue line) or a temperature (laser) pulse (red line).

in the evaporation rate for any material regardless of electrical conductivity[21]. Unlike the case of laser ionization mass analysis (LIMA), the temperature rises involved in laser-pulsed APT are small: typically 100–200 K[22,23]. Data from Kellogg[22] (Fig. 4) shows that, for a given evaporation rate, the evaporation field decreases as the temperature is increased. Between pulses, the voltage should be low enough to prevent dc evaporation and loss of material (shown by a green dot). Voltage pulsing generates field evaporation at a constant temperature by raising the applied field (blue line). However, a laser pulse can generate field evaporation at a constant field by raising the temperature (red line). There is evidence that very short laser pulses (subpicosecond) can also produce increases in the applied field, by a mechanism called optical rectification, generating field evaporation with a lower (or even minimal) temperature rise at the specimen apex[24].

Early experiments performed in the 1980s showed the promise of laser pulsing for studying semiconductor materials problems[25–28], but the additional complexity in both instrument design and use prevented it from becoming mainstream. The advent of faster laser systems and well-engineered commercial 3DAP instruments[29,30] has made laser-pulsed operation as easy as voltage pulsing. Laser pulsing opens a broad universe of applications available for study by atom probe, such as Si and compound semiconductors, multilayer thin films, and even organics[31]. However, even with laser pulsing, the application of APT to a range of materials problems requires the fabrication of a specimen that contains a small region of interest, often from the near-surface region of a substrate wafer, within the apex.

Specimen preparation

Electropolishing has traditionally been used to fabricate the needle-shaped specimen geometry required for atom probe analysis[1]. FIB instruments, often combined with scanning electron microscope facilities in dual-beam systems, provide an alternative method for the fabrication of specimens from site specific regions in a variety of applications. Initial efforts to use higher energy scanned-beam ion milling to prepare atom probe specimens[32,33] had only limited success because of the large spot size and poor resolution of these instruments. Over the last decade, however, the advanced capabilities and the spread of FIB instruments into most microscopy laboratories has led to the development of a wide range of FIB-based techniques for the preparation of atom probe specimens[5,34–36]. FIB milling has been used for a variety of applications including TiAl and CuCo alloys[37], grain boundaries[38–41], alloy powders and ribbons[42], bulk metallic glasses[43], cemented carbides[44], multilayered films[45–47], and Si-based structures and devices[48,49].

FIB milling may now be used to prepare specimens from materials that are difficult to electropolish, to select a specific orientation in a specimen, and to select microstructural features such as coarse or low volume fraction precipitates, grain boundaries, or interphase interfaces. Use of FIB milling allows specimens to be prepared from close to the surface of a material (such as implanted regions, thin films, and electronic devices), greatly expanding the range of materials problems accessible to APT. The most advanced and flexible method of FIB specimen preparation for the atom probe is a site-specific technique, very similar to the 'lift-out' method used routinely for sample preparation in TEM[50]. The individual steps in this method are illustrated in Fig. 5. A thin sheet or bar of material is FIB milled from the surface, (Fig. 5a), a micromanipulator attached (Fig. 5b) and used to remove the sheet (Fig. 5c)[51]. The sheet is attached to a support post, Fig. 5d. At this stage it is possible to cut off the remainder of the sheet and, if appropriate, mount more of the material onto different support posts. Use of an array of microposts for the support allows rapid production of many specimens for subsequent analysis in a LEAP. An annular milling pattern[34] is used to sharpen the specimen to an end radius of <100 nm such that the region of interest is positioned a few tens of nanometers below the apex. An example is shown in Figs. 5e and 5f for a transistor test structure[43].

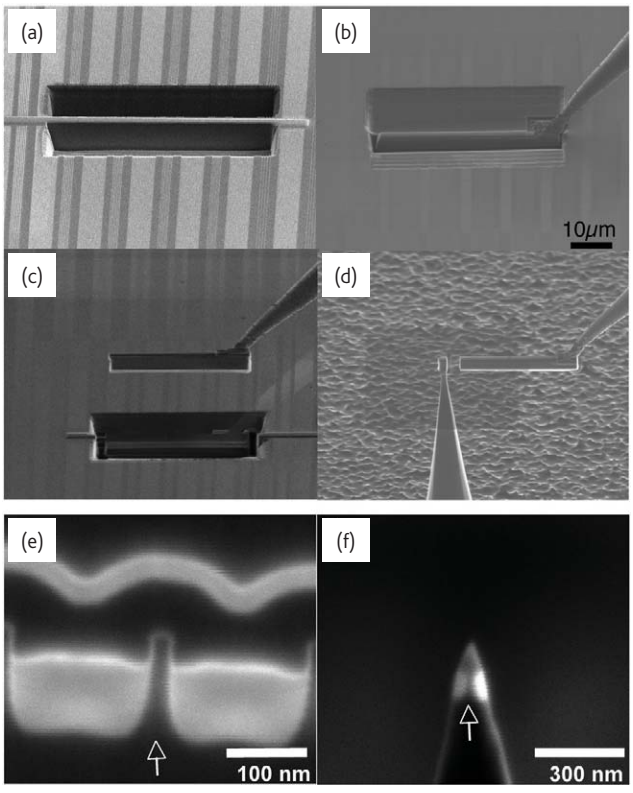

Fig. 5 (a)–(d) Sequence of steps used in the FIB-based technique for specimen preparation. (e),(f) Example of a field-effect transistor structure (e) being sampled using this technique, such that an atom probe specimen is successfully produced (f) containing the gate region within the apex (arrowed).

The remainder of this review gives examples where the use of FIB-based specimen preparation techniques, often combined with laser pulsing, has allowed study of materials problems that would not otherwise been accessible to APT investigation. Of course, this is only a small sample of the applications of APT – a more detailed review of applications to the analysis of electronic materials, for example, can be found elsewhere[52].

Chemistry in the vicinity of a crack-tip

Predicting stress corrosion cracking (SCC) is not an easy task. Currently, the only way to be sure that any particular alloy is not susceptible to SCC in any particular environment is to obtain actual experimental data under those conditions. SCC has been traditionally investigated using indirect methods, either because the available techniques did not have enough resolution or because the region of interest (crack tip) was not accessible for higher resolution techniques such as TEM or APT. Study of the crack tip is critical, since it provides information on the crack advance. Only recently have modern sample preparation techniques allowed characterization of the crack tip region[53,54].

Fig. 6 shows a combined TEM, nanoSIMS, and APT investigation of a type-304, Japanese-grade stainless steel (SUS304) widely used in pressurized water reactors (PWRs). The alloy composition was 0.06 C, 0.5 Si, 1.5 Mn, 0.002 P, 0.001 S, 10 Ni, 15 Cr, <0.01 Mo, and Fe balance (wt.%). The alloy was solution treated at 1060°C for 100 min and water quenched, before cold rolling to a 20% reduction prior to testing. A SCC test (constant load, simulated PWR primary water chemistry at 320°C) lasted 666 hrs and produced intergranular cracks over 100 μm in length. Similar tests have shown a clear correlation between the level of cold work and the crack growth rate[55]. Cold work is known to harden the material through changes in the microstructure such as the formation of deformation shear bands. However, the mechanisms that control crack propagation in cold-worked samples are not yet clear.

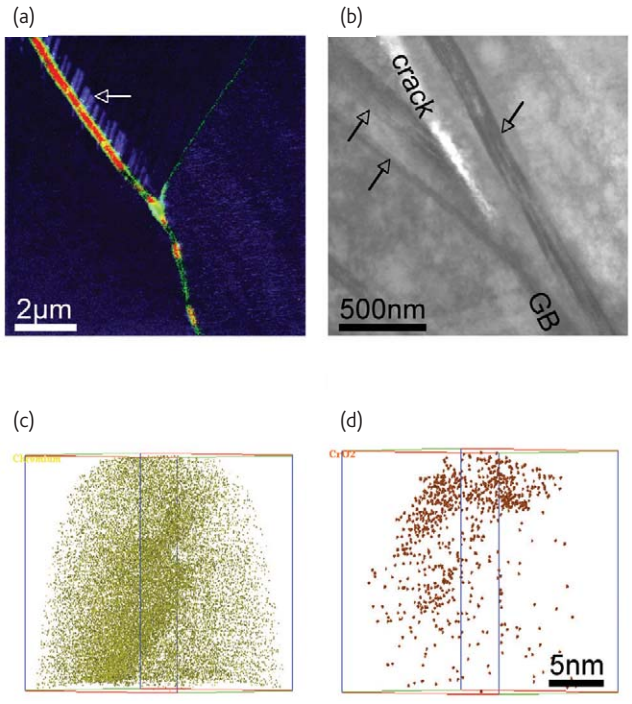

Fig. 6 Study of cracks in a type-304 stainless steel after stress-corrosion cracking. (a) NanoSIMS composite map of the distribution of $^{56}Fe^{16}O^-$ (red), $^{52}Cr^{16}O^-$ (blue), and $^{11}B^{16}O_2^-$ (green) showing oxidized deformation shear bands (arrowed). (b) Bright-field TEM image showing two orientations of shear bands (arrowed) either side of an advancing crack. APT maps of (c) Cr and (d) CrO species from a volume taken from the vicinity of a crack tip, showing O diffusion along a serrated, Cr-segregated shear band.

Surface techniques such as scanning auger microscopy and nanoSIMS[56] have reached the resolution required to extract information on the oxide layer thickness, oxide type, or oxygen penetration depth. More importantly, nanoSIMS adds the possibility of mapping minor segregants such as B or P in concentrations as small as a few parts per million. In Fig. 6a, a region containing a crack tip has been mapped, clearly showing different oxides within the crack, oxidation of shear bands, and B segregation to a grain boundary. However, nanoSIMS is limited by having a maximum lateral resolution of ≈50 nm. TEM can offer information on the microstructure, as can be seen in Fig. 6b, where the different orientations of the shear bands in the grains either side of an intergranular crack are clearly visible, but the chemical information is typically limited to concentrations above 0.1 wt.%[57]. APT can offer three-dimensional mapping with atomic resolution and also detect any minor impurities.

FIB techniques were used to cut out a volume of material at a crack tip and form a sharp specimen for APT. Figs. 6c and 6d show the analysis of a region containing an oxidized shear band that has been in contact with the grain boundary plane followed by the crack (above the analyzed region). The presence of the shear band is shown by the pattern of Cr segregation (Fig. 6c), which indicates a serrated band, as previously observed in TEM[58]. Oxygen is seen to have diffused along the shear band plane, with a very obvious gradient in concentration with distance from the grain boundary (Fig. 6d). Clearly, the deformation shear bands can act as easy diffusion paths for oxygen and Fe, locally accelerating the oxidation rate. Atom-probe analysis allows measurement of diffused oxygen down to <100 ppm levels, at ultrahigh spatial resolution. This type of data will contribute to clarifying the operating mechanisms in SCC of cold-worked materials, as well as providing information on the diffusion coefficients of oxygen down grain boundaries or shear bands at low temperatures.

Atomic-scale dopant mapping

The ever-decreasing size of microelectronic devices, especially for computing applications, has made high-resolution chemical mapping crucial to the development of next-generation integrated circuits. In particular, the mapping of dopant distributions with high spatial resolution has been recognized as an important part of the roadmap for the design of future transistors[59]. APT could provide the required three-dimensional dopant mapping with subnanometer spatial resolution, if it could be shown to be accurate by comparison with existing industry standards, SIMS in particular. Fig. 7a shows just such a direct comparison between SIMS and APT of an undoped <100> Si wafer implanted with 2 x 10^{15} As atoms/cm^2 at an accelerating energy of 30 keV[49]. The wafer was tilted at 7° to avoid channeling

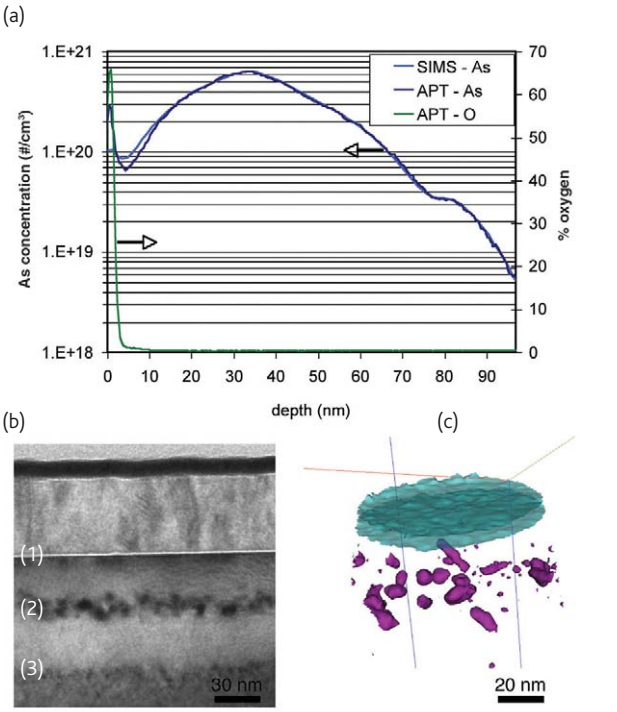

Fig. 7 (a) One-dimensional concentration profile of As (APT and SIMS) and O (APT) from an As-implanted and oxidized Si wafer. (b) Cross section TEM of structure showing oxide layer (1), As-rich defects (2), and end-of-range damage (3). (c) APT reconstruction showing isoconcentration surfaces drawn at 2 at.% As (magenta) and 10 at.% O (cyan).

during the implant. A 2 nm SiO_2 layer was then formed on the surface of the wafer, followed by the deposition of 50 nm of undoped polycrystalline Si (poly-Si). The poly-Si deposition occurs at 600°C and takes approximately 30 mins. The concentration profiles from SIMS and APT analysis of the calibration sample are overlaid in Fig. 7a, showing excellent agreement between the two techniques. The 2 nm thick native oxide is apparent in the atom probe measurement, which also shows As segregation to the oxide; this is less clear in the SIMS profile because of the lower depth resolution of this technique[60].

A cross-sectional TEM image of the implanted wafer shows the microstructure in more detail (Fig. 7b). In particular, dark circular regions are observed at a depth of 35 nm, where the As concentration is seen to reach a peak of 6 x 10^{20}/cm^3 (Fig. 7a). Clearly, these regions are due to As-rich defects. A three-dimensional reconstruction of these regions from the APT data is shown in Fig. 7c. Knowledge of the atom identities and locations allows the construction of isoconcentration surfaces enclosing volumes of material where the local concentration is above some set value. In this case, an O isosurface is constructed at 10 at.% O, which highlights the surface oxide. Isoconcentration surfaces may similarly be drawn with respect to the implanted As atoms, in this case at an As concentration of 2 at.%, to highlight the As-rich regions. From the high-resolution three-dimensional images, these defects are seen to be mostly spheroidal, but some of the defects have already started to evolve into dislocation loops[61] and appear plate-shaped, consistent with further TEM work[49]. These results show that APT is capable of three-dimensional dopant mapping at very high resolution, and in combination with SIMS and TEM can produce a comprehensive, in-depth picture of the dopant distributions.

InGaN/GaN quantum well structures

GaN is one of the most technologically important optoelectronic materials, with a wide range of commercial applications. By alloying it with InN to form $In_xGa_{1-x}N$, or with Al to form $Al_yGa_{1-y}N$, it is possible to produce materials emitting across a wide range of the spectrum, from the green to the ultraviolet. In particular, alternating layers of materials with differing compositions, and hence bandgap, may be used to make multiple quantum wells (MQWs), and such structures form the emissive regions of light-emitting and laser diodes.

There is strong evidence that the carriers are laterally localized within the $In_xGa_{1-x}N$ quantum wells (QWs) on a length scale of 2–5 nm, which allows light emission with high efficiency despite the presence of high densities of threading dislocations[62]. This localization is probably the result of local variations in bandgap causing local energy minima in which the carriers are trapped and prevented from diffusing to the dislocations. On examination of these structures by TEM, it is often reported that there are 2–5 nm regions of strain contrast within the $In_xGa_{1-x}N$ QWs. These regions have been interpreted as regions of high In content, with In fractions reported of $x > 0.7$ or even pure InN[63,64]. Such 'In-rich clusters' would create local

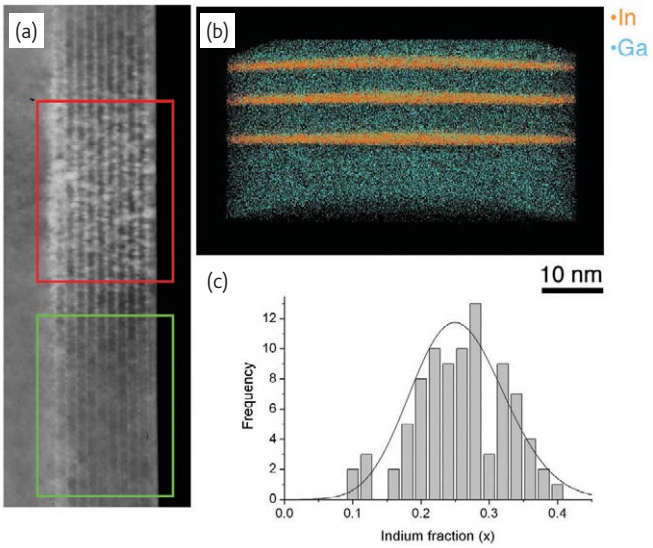

Fig. 8 A comparison of the analysis of possible In clustering in GaInN quantum wells (QWs) by (a) TEM, where the red region has been damaged by exposure to the electron beam, and (b) atom probe, where the QW layers are clearly visualized. (c) Statistical anaylsis of the In distribution in the atom probe data shows that there is excellent agreement between the expected distribution for a random alloy (solid line) and the experimental data (histogram).

energy minima and could be responsible for the carrier localization. However, when such samples were examined in the TEM with very short exposure times to the electron beam, very little strain contrast was observed, with the contrast developing rapidly with further exposure to the electron beam[65]. In Fig. 8a, the region of the image in the red box has been exposed to the 200 kV electron beam for ~60 s, while the region in the green box has been exposed to the beam only very briefly. The In-rich clusters are only present in the exposed region of the sample.

However, it is very hard in the TEM to distinguish between instrumental noise, random alloy fluctuations, and genuine low-level clustering, even if the sample is not damaged by the beam. The atom probe is an ideal instrument to address the issue of In clustering, as it gives direct chemical information about individual atoms, as well as three-dimensional information about their position. Also, as the atom probe does not use high-energy electrons, the sample will not suffer electron-beam damage. Fig. 8b shows the results from the APT analysis of a green-emitting $In_xGa_{1-x}N$/GaN MQW structure consisting of 2.4 nm QWs, with a composition of $x = 0.23$, separated by 7.0 nm GaN spacer layers. Three of the QWs are clearly visible in the reconstruction of Fig. 8b. Data from within the QWs was divided into approximately cubic blocks containing 100 atoms and the In content of each block calculated. The distribution of In concentration in the experimental data (Fig. 8c) was found to have no significant deviation from the binomial distribution that would be expected for a random alloy. A comparison of the measured In distribution with that expected for a random alloy in Fig. 8c shows a good match, and this is confirmed

quantitatively with a χ^2 test. The same result is obtained for a sample emitting in the blue part of the spectrum[66]. There is, therefore, no evidence for any In clustering. Since both these samples give typical light emission without clustering, we conclude that In clustering is not essential for luminescence in $In_xGa_{1-x}N$/GaN structures. This represents a fundamental change in our understanding of the mechanism of luminescence in this important materials system, and should help in the design and production of improved devices.

Conclusions

The development of advanced specimen preparation techniques combined with the advent of laser-pulsed field evaporation has revolutionized the field of atom probe research, expanding its capabilities into a wide variety of new applications fields. The examples given in this review show how APT can now be used to study the chemistry at specific features in engineering alloys, to map accurately the three-dimensional dopant concentrations in semiconductor devices, and to characterize semiconductor heterostructures. In these and other areas, the atomic-resolution chemical mapping of APT is capable of providing information not available by any other technique and hence giving valuable insights into materials problems, new and old. mt

Acknowledgments

The Opal National Atom Probe Facility is funded by the UK Engineering and Physical Sciences Research Council (EPSRC) under grant number EP/077664/1. AC would like to thank Imago Scientific Instruments for funding during the preparation of this paper, and SL-P is grateful to INSS (Japan) for sponsoring the research on crack-tip chemistry. LEAP is a trademark of Imago Scientific Instruments.

REFERENCES

1. Miller, M. K., *et al.*, *Atom probe field-ion microscopy*, Oxford University Press, Oxford, (1996)
2. Cerezo, A., *et al.*, *Rev. Sci. Instrum.* (1988) **59**, 862
3. Blavette D., *et al. Rev. Sci. Instrum.* (1993) **64**, 2911
4. Miller, M. K., *Atom probe tomography*, Plenum Press, New York, (2000)
5. Miller, M. K., *et al.*, *Ultramicroscopy* (2005) **102**, 287
6. Thompson, K., *et al.*, *Appl. Phys. Lett.* (2005) **87**, 052108
7. Liddle, J. A., *et al.*, *Appl. Phys. Lett.* (1989) **54**, 1555
8. Gault, B., *et al.*, *Rev. Sci. Instrum.* (2006) **77**, 043705
9. Bunton, J. H., *et al.*, *Microsc. Microanal.* (2006) **12** (Suppl. 2), 1730CD
10. Shared Research Equipment User Facility (ShaRE), Oak Ridge National Laboratory, www.ornl.gov/share
11. Northwestern University Centre for Atom Probe Tomography, arc.nucapt.northwestern.edu
12. Opal UK National Atom Probe Facility, www.materials.ox.ac.uk/fim/opal.html
13. Müller, E. W., *et al.*, *Rev. Sci. Instrum.* (1968) **39**, 83
14. Nishikawa, O., and Kimoto, M., *Appl. Surf. Sci.* (1994) **76–77**, 424
15. Kelly, T. F., *et al.*, *Microsc. Microanal.* (2004) **10**, 373
16. Vaumousse, D., *et al.*, *Ultramicroscopy* (2003) **95**, 215
17. Edwards, G. A., *et al.*, *Acta Mater.* (1998) **46**, 3893
18. Murayama, M., *et al.*, *Metall. Mater. Trans. A* (2001) **32**, 239
19. De Geuser, F., *et al.*, *Philos. Mag. Lett.* (2006) **86**, 227
20. Buha, J., *et al.*, *Acta Mater.* (2007) **55**, 3015
21. Kellogg, G. L., and Tsong, T. T., *J. Appl. Phys.* (1980) **51**, 1184
22. Kellogg, G. L., *J. Appl. Phys.* (1981) **52**, 5320
23. Cerezo, A., *et al.*, *J. Microsc.* (1986) **141**, 155
24. Vella, A., *et al.*, *Phys. Rev. B* (2006) **73**, 165416
25. Cerezo, A., *et al.*, *J. Microsc.* (1986) **141**, 155
26. Grovenor, C. R. M., and Cerezo, A., *J. Appl. Phys.* (1989) **65**, 5089
27. Liddle, J. A., *et al.*, *Appl. Phys. Lett.* (1989) **54**, 1555
28. Mackenzie, R. A. D., *et al.*, *J. Appl. Phys.* (1991) **69**, 250
29. Imago Scientific Instruments, www.imago.com/imago/html/products/products.jsp
30. CAMECA, www.cameca.fr/html/product_atom_probe.html
31. Prosa, T., *et al.*, unpublished data
32. Waugh, A. R., *et al.*, *J. Phys.* (1984) **45-C9**, 207
33. Alexander, K. B., *et al.*, *J. Phys.* (1989) **50-C8**, 549
34. Larson, D. J., *et al.*, *Ultramicroscopy* (1999) **79**, 287
35. Larson, D. J., *et al.*, *Microsc. Microanal.* (2001) **7**, 24
36. Thompson, K., *et al.*, *Ultramicroscopy* (2006) **107**, 131
37. Larson, D. J., *et al.*, *Ultramicroscopy* (1998) **75**, 147
38. Seto, K., *et al.*, *Scripta Mater.* (1999) **40**, 1029
39. Lawrence, D., *et al.*, *Microsc. Microanal.* (2006) **12** (S2), 1740
40. Takahashi, J., *et al.*, *Ultramicroscopy* (2007) **107**, 744
41. Cairney, J. M., *et al.*, *Physica B* (2007) **394**, 267
42. Miller, M. K., and Russell, K. F., *Ultramicroscopy* (2007) **107**, 761
43. Miller, M. K., *et al.*, *Microsc. Microanal.* (2007), doi: 10.1017/S1431927607070845
44. Östberg, G., and Andrén, H.-O., *Metall. Mater. Trans. A* (2006) **37**, 1495
45. Larson, D. J., *et al.*, *Appl. Phys. Lett.* (2000) **77**, 726
46. Thompson, G. B., *et al.*, *Acta Mater.* (2003) **51**, 5285
47. Tamion A., *et al.*, *Scripta Mater.* (2006) **54**, 671
48. Thompson, K., *et al.*, *Solid State Technol.* (June 2006), 65
49. Thompson, K., *et al.*, *Science* (2007) **317**, 1370
50. Mayer, J., *et al.*, *MRS Bull.* (2007) **32** (5), 400
51. Miller, M. K., *et al.*, *Ultramicroscopy* (2005) **102**, 287
52. Kelly, T. F., *et al.*, *Annu. Rev. Mater. Res.* (2007) **37**, 681
53. Arioka, K., *et al.*, *Corrosion* (2006) **62**, 74
54. Lozano-Perez, S., and Titchmarsh, J. M., *Mater. High Temp.* (2003) **20**, 573
55. Arioka, K., *et al.*, *Corrosion* (2006) **62**, 568
56. Lozano-Perez, S., *et al.*, *J. Nucl. Mater.* (2007), doi: 10.1016/j.jnucmat.2007.07.009
57. Watanabe, M., and Williams, D., *Microsc. Microanal.* (2005) **11** (Suppl. 02), 1362
58. Fukuya, K., *et al.*, In: *Proceedings of the 12th International Conference on Environmental Degradation of Materials in Nuclear Power Systems: Water Reactors*, Allen, T. R., *et al.*, (eds.), The Minerals, Metals & Materials Society, Warrendale, PA, USA (2006), 389
59. International Technology Roadmap for Semiconductors, www.src.org
60. Vandervorst, W., *et al.*, *Appl. Surf. Sci.* (2004) **231–232**, 618
61. Basu, D., *et al.*, *J. Vac. Sci. Technol. B* (2006) **24**, 2424
62. Graham, D. M., *et al.*, *J. Appl. Phys.* (2005) **97**, 103508
63. Gerthsen, D., *et al.*, *Phys. Status Solidi A* (2000)**177**, 145
64. Ruterana, P., *et al.*, *J. Appl. Phys.* (2002) **91**, 8979
65. Smeeton, T. M., *et al.*, *J. Mater. Sci.* (2006) **41**, 2729
66. Galtrey, M. J., *et al.*, *Appl. Phys. Lett.* (2007) **90**, 061903